

Improved Quantum Supersampling for Quantum Ray Tracing

Xi Lu^{1,2} and Hongwei Lin^{1,2}

¹School of Mathematical Science, Zhejiang University, Hangzhou, 310027, China

²State Key Lab. of CAD&CG, Zhejiang University, Hangzhou, 310058, China

Abstract

Ray tracing algorithm is a category of rendering algorithms that calculate the color of pixels by simulating the physical movements of a huge amount of rays and calculating their energies, which can be implemented in parallel. Meanwhile, the superposition and entanglement property make quantum computing a natural fit for parallel tasks. Here comes an interesting question, is the inherently parallel quantum computing able to speed up the inherently parallel ray tracing algorithm? The ray tracing problem can be regarded as a high-dimensional numerical integration problem. Suppose N queries are used, classical Monte Carlo approaches has an error convergence of $O(1/\sqrt{N})$, while the quantum supersampling algorithm can achieve an error convergence of approximately $O(1/N)$. However, the outputs of the origin form of quantum supersampling obeys a probability distribution that has a long tail, which shows up as many detached abnormal noisy dots on images. In this paper, we improve quantum supersampling by replacing the QFT-based phase estimation in quantum supersampling with a robust quantum counting scheme, the QFT-based adaptive Bayesian phase estimation. We quantitatively study and compare the performances of different quantum counting schemes. Finally, we do simulation experiments to show that the quantum ray tracing with improved quantum supersampling does perform better than classical path tracing algorithm as well as the original form of quantum supersampling.

CCS Concepts

• *Computer systems organization* → *Quantum computing*; • *Computing methodologies* → *Ray tracing*;

1. Introduction

Ray tracing [Whi80, CPC84, Kaj86, HAM19] is a general term of rendering algorithms that calculate pixel colors by simulating all the physical interactions between light rays and the scene. Since a single ray scatters towards many directions when interacting with an object, and each of the scattered rays scatters towards more directions when interacting with other objects, the total number of rays grow exponentially in the number of interactions. A standard solution to this problem is Monte Carlo ray tracing, or *path tracing* [Kaj86], which randomly shoots only one ray at each bounce. To render an image with high quality, path tracing algorithm require many rays to reduce noise. In many situations people have to make a trade-off between time cost and quality. For real-time ray tracing applications where the rendering time is strictly limited, the state-of-the-art GPU can only handle sampling a small amount of rays per pixel, and the quality of result relies heavily on subsequent denoising procedures [AMHH18, ZLY*21, SKW*17]. Therefore, a major problem in ray tracing is to reduce the time cost while maintaining the quality.

Quantum computing [NC02] is an emerging subject that studies how to perform computational tasks in quantum mechanical systems. By leveraging the superposition and entanglement of quantum computing, quantum computing has inherent advantages

on parallel computational tasks. As a result, quantum computing shows its computational power by providing spectacular speedup over classical computing in some problems [Gro97, Sho97].

The idea of introducing quantum computing into computer graphics was early proposed in 2005 [LU05], which raises many concepts such as quantum Z-buffer, ray tracing and radiosity algorithm. Later, Caraiman [Car12] introduced quantum solutions for the polygon visibility and global illumination problems and developed the appropriate quantum algorithms. In both articles, quantum speedup comes from the superposition of all scene primitives. Johnson [Joh16] proposed quantum supersampling as the quantum variant of Monte Carlo integration in ray tracing, and did simulation experiments on binary image filtering to show that quantum supersampling can reduce mean pixel error faster. Shimada et al. [SH20] also did experiments on binary image filtering using quantum coin (QCoin) method originally proposed in [AW99]. Recently Santoset al. [SBRBN22] investigated on using quantum computing for intersection searching subroutine in ray tracing, which provides a quadratic complexity in scene complexity.

There are generally two potential approaches for quantum speedup in ray tracing algorithm. One is to store the scene primitives in a superposition and apply quantum minimum search [DH96] to find the nearest intersection between each ray

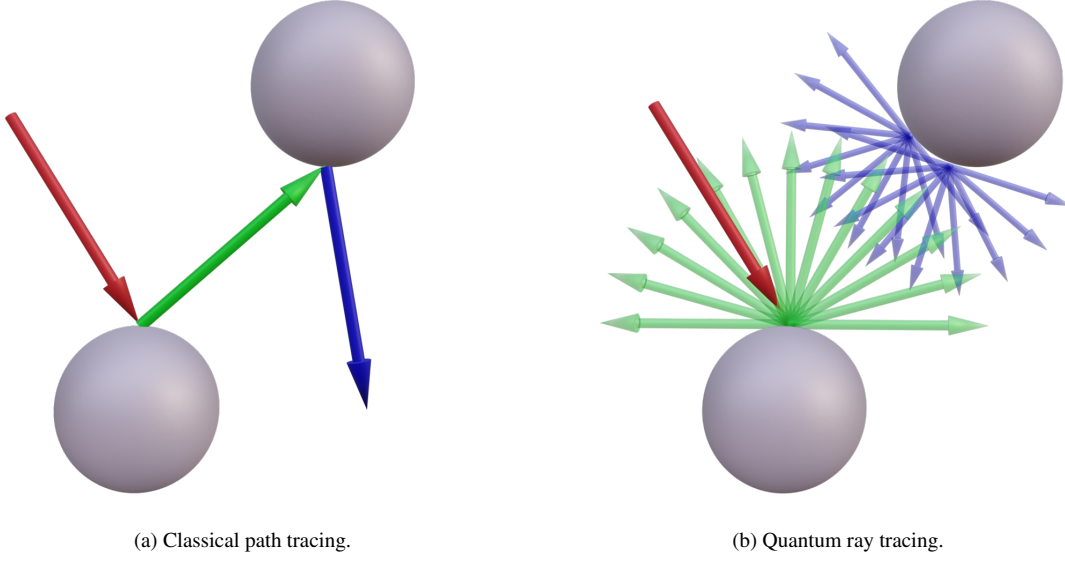


Figure 1: Classical path tracing only traces one ray at a time, while quantum ray tracing can trace numerous rays as a superposition in one shot.

and the scene, to obtain a quadratic speedup, as well studied in [SBRBN22]. The other is to store the ray paths in a superposition, as illustrated in Fig. 1, such that an astronomical amount of rays, at the cost of a logarithmic space and time, can be traced simultaneously to reduce error. Plus, we do not have the same worry as the first approach, since the rays are procedurally generated instead of reading from classical memory. This approach is used in quantum supersampling and quantum coin method.

As is shown in [Joh16], the image produced by quantum supersampling (QSS) contains many detached noisy dots. In this paper, we improve quantum supersampling for quantum ray tracing, by replacing the standard quantum Fourier transformation (QFT) based phase estimation algorithm (QFT-PEA) with more robust quantum counting schemes. The quality of the output image relies dominantly on the quantum counting scheme. For example, the quantum counting scheme used in QSS is the standard QFT-PEA, which outputs a random variable that is concentrated in a vicinity of the ground truth, but has a long tail in the meantime. We quantitatively analyze the performances of different quantum counting schemes. We also propose the QFT-based adaptive Bayesian phase estimation (QFT-ABPEA) as a substitute for QFT-PEA in QSS.

Finally, we build a 3D scene, use a large enough number of samples with the *Blender cycles* renderer to generate the ground truth, and simulate the quantum noise by sampling random numbers from the theoretical distribution, to simulate the quantum ray tracing result. We also use a limited number of samples with *Blender cycles* as a representation of classical path tracing result, and show that quantum ray tracing does perform better than classical ray tracing, conditioned on similar computational cost.

Our contributions are as follows.

- Analyze the performances of some existing quantum counting

schemes that are potential substitutes of QFT-based phase estimation algorithm in QSS.

- Propose a QFT-based adaptive Bayesian phase estimation algorithm.
- Apply improved QSS to ray tracing algorithm. Do experiments that simulate the workflow of ray tracing, and simulate the images rendered by classical and quantum ray tracing to prove that quantum ray tracing does have better visual performance over classical ray tracing, if appropriate quantum counting scheme is used.

The structure of the paper is as follows. In Section 2 we present basic knowledge about quantum computing, including fundamental concepts, quantum phase estimation and quantum counting. In Section 3, we present a framework for quantum ray tracing, analyze the performances of several schemes and propose a QFT-based adaptive Bayesian phase estimation scheme. Then in Section 4, we do some simulation experiments on real images rendered by classical ray tracing, QCoin, and QSS with different schemes, to show that improved QSS does have a better visual performance than classical ray tracing, the original form of QSS and QCoin method, conditioned on the same computational cost. In Section 5 and Section 6, we make some discussions and conclusions.

2. Preliminary

2.1. Fundamental concepts of Quantum Computing

All stories began in the 1980s when Feynman suggested that quantum mechanics might be more computationally powerful than Turing machine in some problems like simulating the physical world [Fey82, Fey86]. By substituting classical bits for quantum bits, or *qubits*, which can be not only in the states $|0\rangle$ and $|1\rangle$ but also their superposition $a|0\rangle + b|1\rangle$ where $a, b \in \mathbb{C}$ and $|a|^2 + |b|^2 =$

1, quantum computing obtains many interesting features like entanglement, reversibility, parallelism, no-cloning and non-orthogonal indistinguishability [NC02].

Quantum computing follows the gate model with three general steps: initializing all qubits into zero state, performing unitary transformations, and finally measuring them to turn quantum information into classical one. Operations on qubits are implemented by *quantum gates*, the quantum variants of classical logic gates. As we know, any classical computing circuit can be constructed with NOT gates, AND gates and COPY gates. Thus, a quantum computer can simulate a classical computer, by restricting the qubit states to $\{|0\rangle, |1\rangle\}$, and using the Toffoli gate, X gate and CNOT gate to replace the AND gate, NOT gate and the COPY gate in classical computers, respectively.

$$\begin{aligned} \text{Toffoli: } |a\rangle |b\rangle |0\rangle &\mapsto |a\rangle |b\rangle |a \text{ and } b\rangle \\ \text{X: } |a\rangle &\mapsto |\text{not } a\rangle \\ \text{CNOT: } |a\rangle |0\rangle &\mapsto |a\rangle |a\rangle \end{aligned}$$

Furthermore, due to the reversibility of the three gates above, the quantum implementation of a classical function $j \mapsto f(j)$ should be of the following form,

$$|j\rangle |0\rangle \mapsto |j\rangle |f(j)\rangle, \quad (1)$$

which we abbreviate as $|j\rangle \mapsto |j\rangle |f(j)\rangle$ throughout this paper. Here $|j\rangle$ and $|f(j)\rangle$ are quantum registers that use several qubits to store various data structures like integers and real numbers. It follows immediately that when a superposition state $\sum_j x_j |j\rangle$ is inputted, where x_j s are arbitrary complex coefficients, the same quantum circuit performs the following linear transformation,

$$\sum_j x_j |j\rangle \mapsto \sum_j x_j |j\rangle |f(j)\rangle, \quad (2)$$

due to the linear property. We call such circuits *quantum linear circuits*. Any classical circuit can be turned into quantum linear circuit in the brute-force way above, though there are works studying more efficient approaches, like quantum circuit for addition and comparison [TTK09].

Though several evaluations of the function f are computed in one query, we cannot read them all out directly. Once we measure the state on the computational basis and get access to a specific $f(j_0)$, the whole state must collapse to the basis state $|j_0\rangle |f(j_0)\rangle$, and the information of other evaluations is lost forever. Anyway, we have to design clever algorithms to make the best use of quantum parallelism. Some of such examples are Grover's search [Gro97], minimum finding [DH96], quantum counting [BHT98], and quantum numerical integrals [AW99].

2.2. Quantum Phase Estimation

Given a quantum circuit that performs unitary transformation U , and an eigenstate $|\psi\rangle$ of U such that

$$U |\psi\rangle = e^{2\pi i \phi} |\psi\rangle, \quad (3)$$

the *phase estimation algorithm* (PEA) [Kit95, Sho97] provides an efficient way to estimate ϕ . For general state $|\psi\rangle$ that is not neces-

sarily an eigenstate, let

$$|\psi\rangle = \sum_j c_j |\psi_j\rangle, \quad (4)$$

be the orthogonal decomposition onto the eigenspaces of U , where $|\psi_j\rangle$ is an eigenstate of U with respect to eigenvalue $e^{2\pi i \phi_j}$, then PEA returns an estimation of ϕ_j with probability $|c_j|^2$. The PEA is considered the source of quantum speedup of the celebrated Shor's integer factorization algorithm [Sho97].

The well-known *Quantum Fourier Transformation* (QFT)-based form of PEA uses the circuit shown in Fig. 2, where $H^{\otimes t}$ gate means applying Hadamard gate to each of the t qubits, QFT^\dagger is the inversed QFT circuit. The number of queries to U is $T - 1$.

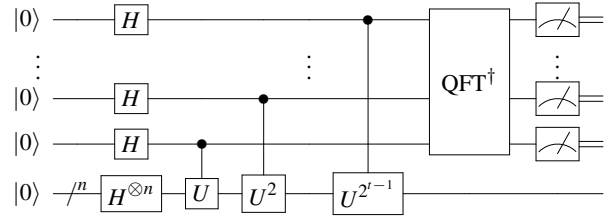


Figure 2: The quantum circuit of QFT-PEA.

From the textbook [NC02] we can find that the output $\tilde{\phi}$ of PEA obeys the following distribution,

$$P(\tilde{\phi}|\phi) = \left(\frac{\sin(T\pi(\tilde{\phi} - \phi))}{T \sin(\pi(\tilde{\phi} - \phi))} \right)^2, \quad (5)$$

where $T = 2^t$ and $\tilde{\phi} \in \{0, 1/T, 2/T, \dots, 1\}$. From Eq. we know that QFT-PEA is accurate when ϕ is an integer multiplication of T^{-1} , and shows the biggest noise when ϕ is a half integer multiplication of T^{-1} . The probability of estimating within accuracy $1/T$ is at least $8/\pi^2$.

The phase estimation problems are sometimes called in a more general name, the amplitude estimation problem. That is, given a unitary transformation $U : |0\rangle \rightarrow \sqrt{1-a^2} |0\rangle + a |1\rangle$, estimate a . The schemes for amplitude estimation are still a research hotspot in recent years [SHF13, WG16, Wie19, SUR*19, GGZW21].

2.3. Quantum Counting Scheme

Given any Boolean function $f : \{0, 1, \dots, N-1\} \rightarrow \{0, 1\}$, where $N = 2^n$ ($n \in \mathbb{Z}_+$), as well as the quantum circuit that performs the transformation,

$$O_f : |j\rangle \mapsto |j\rangle |f(j)\rangle, \quad (j = 0, 1, \dots, N-1) \quad (6)$$

the quantum counting algorithm [BHT98] can estimate the sum $S = \sum_{j=0}^{N-1} f(j)$ with a quadratic faster convergence rate over classical Monte Carlo counting.

The key idea of quantum counting is to construct a unitary transformation whose eigenvalue contains information about S . The celebrated Grover's iteration [Gro97] is exactly such a unitary trans-

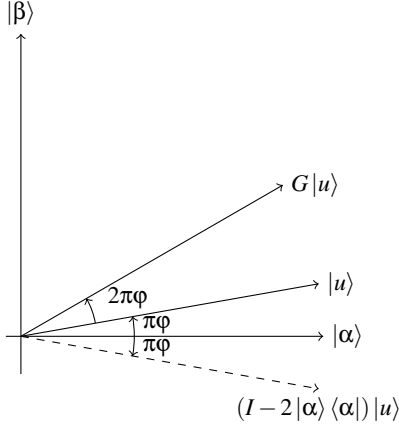


Figure 3: An illustration of Grover's iteration.

formation. Let

$$|\alpha\rangle = \frac{1}{\sqrt{N-S}} \sum_{f(j)=0} |j\rangle, \quad (7)$$

$$|\beta\rangle = \frac{1}{\sqrt{S}} \sum_{f(j)=1} |j\rangle, \quad (8)$$

$$|u\rangle = \frac{1}{\sqrt{N}} \sum_{j=0}^{N-1} |j\rangle. \quad (9)$$

As illustrated in Fig. 3, a Grover's iteration [Gro97] G consists of two reflections, one about $|\alpha\rangle$ and the other about $|u\rangle$, that is,

$$\begin{aligned} G &= (I - 2|u\rangle\langle u|)(I - 2|\alpha\rangle\langle\alpha|) \\ &= H^{\otimes n} O_0 H^{\otimes n} P_f, \end{aligned} \quad (10)$$

where

$$O_0 = I - 2|0\rangle\langle 0|, \quad (11)$$

and $H^{\otimes n}$ is to apply Hadamard transformation to each of the n qubits, and P_f is called the phase oracle of O_f which performs the transformation,

$$P_f : \sum_j x_j |j\rangle \mapsto \sum_j (-1)^{f(j)} x_j |j\rangle. \quad (12)$$

Therefore, U acts as a rotation by twice the angle between $|u\rangle$ and $|\alpha\rangle$ on the plane spanned by $\{|\alpha\rangle, |\beta\rangle\}$. When restricted in this plane, the eigenvalues of such a plane rotation is $e^{\pm 2\pi i \varphi}$ ($0 \leq \varphi < 1/2$), where

$$\sin(\pi\varphi) = \sqrt{\frac{S}{N}}, \quad (13)$$

is the rotation angle, and the corresponding eigenstates are

$$|\Psi_{\pm}\rangle = \frac{1}{\sqrt{2}}(|\alpha\rangle \mp i|\beta\rangle). \quad (14)$$

Since

$$|u\rangle = e^{i\pi\varphi} |\Psi_+\rangle + e^{-i\pi\varphi} |\Psi_-\rangle, \quad (15)$$

we can defer that when applying PEA to U with quantum state $|u\rangle$, we can get the output φ or $1 - \varphi$ with equal probability. We can easily distinguish them, as $0 \leq \varphi < \frac{1}{2}$. From Eq. (2.2) we see the quantum counting result obeys the random distribution,

$$P(\tilde{\varphi}|\varphi) = \begin{cases} \left(\frac{\sin(T\pi(\tilde{\varphi}-\varphi))}{T \sin(\pi(\tilde{\varphi}-\varphi))} \right)^2 + \left(\frac{\sin(T\pi(\tilde{\varphi}+\varphi))}{T \sin(\pi(\tilde{\varphi}+\varphi))} \right)^2, & \tilde{\varphi} = \frac{1}{T}, \frac{2}{T}, \dots, \frac{1}{2} - \frac{1}{T}; \\ \left(\frac{\sin(T\pi(\tilde{\varphi}-\varphi))}{T \sin(\pi(\tilde{\varphi}-\varphi))} \right)^2, & \tilde{\varphi} = 0, \frac{1}{2}. \end{cases} \quad (16)$$

Another approach is the *Amplitude Amplification* (AA), which uses Grover's iteration as amplitude amplification, and the information about amplitude is extracted via repeated direct measurements. For example, by applying O_f directly to the uniform superposition state $|u\rangle$ we obtain $\frac{1}{\sqrt{N}} \sum_j |j\rangle |f(j)\rangle$, so the measurement on the second register will output 1 with probability $\sin^2(\pi\varphi) = S/N$. If M times of Grover's iteration is applied to $|u\rangle$ before measurement, the probability becomes $\sin^2((2M+1)\pi\varphi)$. With well-designed schemes like [AW99, SUR*19, AR20] the information about φ can also be extracted with high precision.

3. Algorithm

When dealing with a numerical integration problem, classical Monte Carlo method randomly evaluates N samples to get an estimation with an error convergence of $1/\sqrt{N}$. In quantum computers, a large range of samples can be made into a superposition state, and thus can be computed in one shot. Based on this idea, Johnson [Joh16] proposed quantum supersampling (QSS), and experimentally proved it to have a faster convergence than Monte Carlo method. However, their result images contain many detached noisy dots that severely affect the quality of image, as they use a non-robust QFT-based phase estimation (QFT-PEA) as the quantum counting scheme. In this section, we present a framework of quantum ray tracing, then propose improved QSS by replacing the QFT-based phase estimation with more robust quantum counting schemes.

3.1. Framework of quantum ray tracing

In classical path tracing, many ray paths are required to calculate the color of a single pixel as accurately as possible. In quantum computing, the information of all those rays can be stored in a superposition. All we need is an extra register that stores the ID of each superposed ray, in the form $\sum_{ID} |ID\rangle |ray_{ID}\rangle$. Moreover, the quantum memory used for storing those IDs uses only a logarithmic space, while the memory used for storing path information like origins and directions is shared in superposition, so the biggest advantage of quantum ray tracing is that we can reduce the sampling error to a negligible level by using an astronomical number of rays.

As is introduced, we can assume that we are given a ray tracing oracle implementing the following transformation,

$$O_f(pixel, channel) : \sum_{j=0}^{N-1} x_j |j\rangle \mapsto \sum_{j=0}^{N-1} x_j |j\rangle |f(j)\rangle, \quad (17)$$

where *pixel* and *channel* (R, G or B) are classical parameters, j

plays the role of ray ID, and $f(j)$ is a real number that stands for the ray energy. In the rest of this paper f is specified as the function that maps ray ID to ray energy. The oracle can trace $N = 2^n$ paths simultaneously, and the final color we hope to write to the corresponding pixel and channel is the average of those energies,

$$S = \frac{1}{N} \sum_{j=0}^{N-1} f(j). \quad (18)$$

Suppose those real numbers $f(j)$ are stored in a fixed-point format with integer bit length b_0 and total bit length b , we can transfer the estimation problem of Eq. (18) into quantum counting by constructing a Boolean function,

$$g(j, k) = \begin{cases} 1, & f(j) \geq 2^{b_0-b}k; \\ 0, & f(j) < 2^{b_0-b}k. \end{cases} \quad (k = 0, 1, \dots, 2^b - 1) \quad (19)$$

The phase oracle O_g for g in Grover's search is,

$$O_g : \sum_{j,k} |j\rangle |k\rangle \mapsto \sum_{j,k} (-1)^{g(j,k)} |j\rangle |k\rangle. \quad (20)$$

To construct O_g , we need a comparison gate that performs the comparison operation $COMP$ on the two integers $2^{b-b_0}f(j)$ and k ,

$$COMP : \sum_{j,k} |f(j)\rangle |k\rangle \mapsto \sum_{j,k} |f(j)\rangle |k\rangle |g(j, k)\rangle, \quad (21)$$

which is already constructed by [TTK09]. With this in hand, the O_g gate can be easily constructed, as shown in Fig. 4.

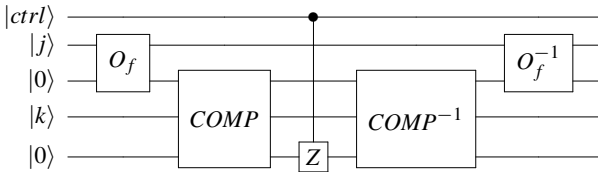


Figure 4: The construction of controlled- O_g , where the first qubit is the control qubit, and $Z : |x\rangle \mapsto (-1)^x |x\rangle$.

It is easy to verify that,

$$S = \frac{1}{2^n} \sum_{j=0}^{N-1} f(j) = \frac{1}{2^{n+b-b_0}} \sum_{j=0}^{N-1} \sum_{k=0}^{2^b-1} g(j, k). \quad (22)$$

Also, the conversion to fixed-point format brings a truncation error of $O(2^{-b}N)$.

Finally, the quantity $\sum_{j,k} g(j, k)$ can be estimated by quantum counting algorithm. The construction of controlled- G_g required in quantum counting is shown in Fig. 5. This is also where the dominant error of the whole procedure is brought.

In the paper we assume one call to O_f in quantum realm takes the same time as tracing one path in classical realm. We evaluate the cost of classical path tracing by the number of ray paths N_c , as the noise comes mostly from the Monte Carlo integration. And in quantum ray tracing, the time cost is evaluated by the number of queries

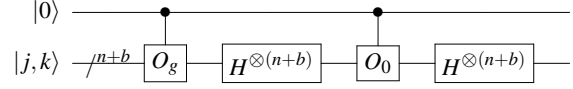


Figure 5: The construction of controlled- G_g gate, where $|j, k\rangle$ is written as an entity of the two registers $|j\rangle$ and $|k\rangle$.

N_q to the ray tracing oracle O_f , and the noise comes mostly from the random distribution of the output of PEA. The QFT-based quantum counting has an error convergence rate of $O(1/N_q)$ [BHT98], hence has a quadratic speedup over classical Monte Carlo integration with convergence rate of $O(1/\sqrt{N_c})$.

Finally, the averaging step of ray energies takes place in the linear *high-dynamic range* (HDR) color space. To obtain a color between range $[0, 1]$ in the *standard-dynamic range* (SDR) space, a tone mapping [Arr17] step should be applied to the averaged color. In summary, the framework of quantum ray tracing is illustrated in Fig. 6.

3.2. Schemes for quantum counting

In many cases, QFT-based phase estimation algorithm (QFT-PEA) is already enough to use. However, from Eq. (2.2) we know $P(\tilde{\phi}|\phi)$ decays with an order of $\sin^{-2}(\pi(\tilde{\phi} - \phi))$ as $|\tilde{\phi} - \phi|$ grows big. That is, though the output $\tilde{\phi}$ of PEA is randomly distributed around the ground truth ϕ , it also has a long tail which shows as many detached noisy dots on the image. That is exactly why the result of the original form of QSS contains many distinct noisy dots.

To have a visual impression on this proposition, we do the experiments on the gray disk with the gray scale varying linearly from black at the center to white on the border, as shown in Fig. 7(b). The gray scale of each pixel stands for S/N in quantum counting. By sampling from the theoretical random distribution of each algorithm, we can simulate the output \tilde{S}/N and draw the gray scale to the corresponding pixel. In Fig. 7, (a) shows the result of Monte Carlo sampling with N samples drawn from the binary distribution as a comparison, (b) shows the result of QFT-PEA, which contains some distinct dots, consistent with long tail phenomenon of Eq. (16).

Intuitively, the noise of QFT-PEA can be reduced by repeating for N_{shot} times and applying Bayesian estimation. That is, finding the maximum of the function,

$$L(\tilde{\phi}) = \prod_{k=1}^{N_{\text{shot}}} P(\theta_k|\tilde{\phi}), \quad (23)$$

where we assume the priori distribution is uniform, $\{\theta_k\}$ are the estimated phases in each trial of PEA, and P is the probability distribution given by Eq. (16). We call this method *QFT-based Bayesian Phase Estimation* (QFT-BPEA) in this paper. The gray disk experiment result is shown in Fig. 7(c). We can see that the noise level of detached distinct dots is obviously reduced. But if we zoom in, Fig. 7(c) shows slight fake rings, because the parameter T in each run of QFT-BPEA is smaller than QFT-PEA. Thus, the fake ring phenomenon guided by Eq. (2.2) in QFT-BPEA is stronger.

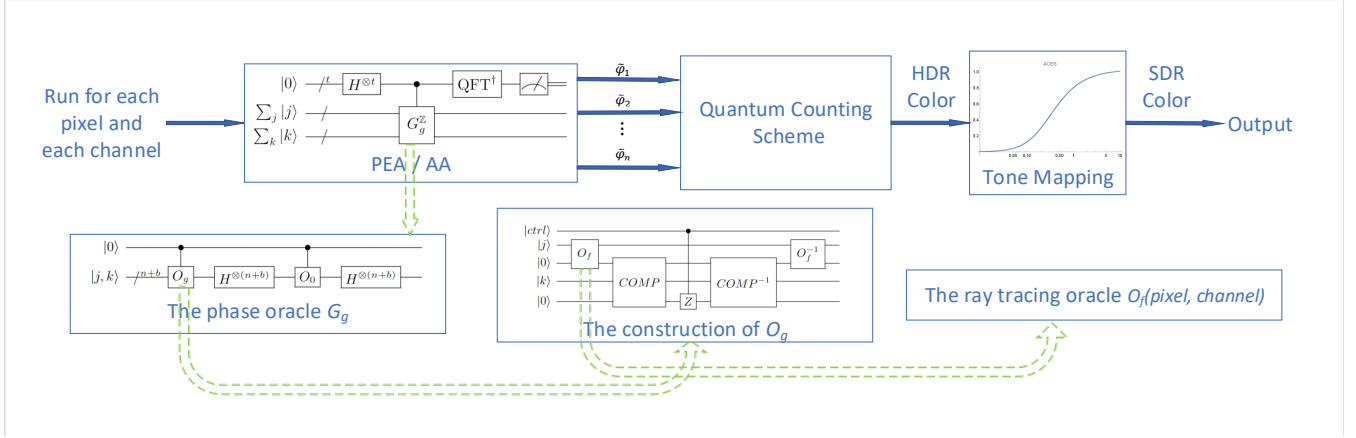


Figure 6: The framework of quantum ray tracing. The quantum counting may use PEA/AA for schemes.

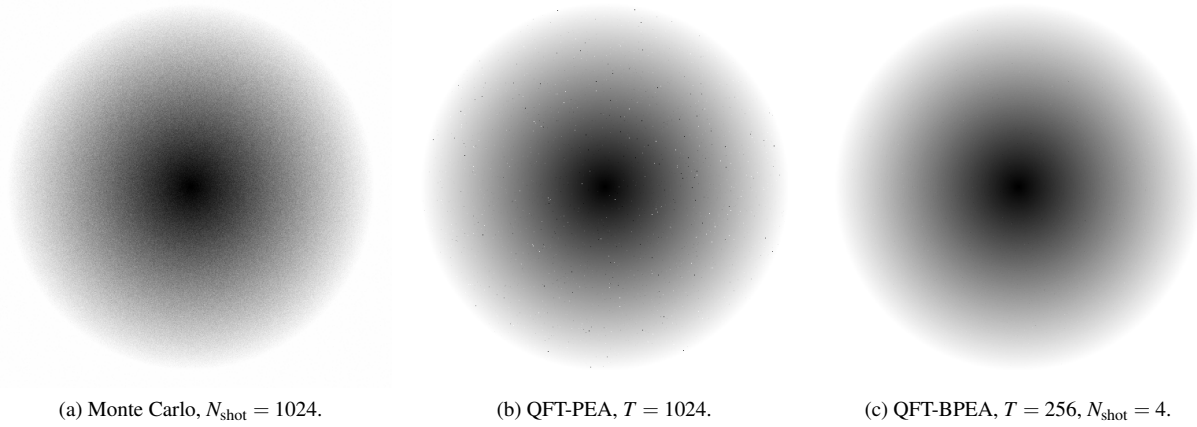


Figure 7: Gray disk experiments.

Based on the observation that about $8/\pi^2$ estimations of PEA are within accuracy $1/T$, we can dynamically adjust N_{shot} until most of the samples are within an interval of length $2/T$. We propose the *QFT-based adaptive Bayesian PEA* (QFT-ABPEA) in Algorithm 1.

Algorithm 1: QFT-ABPEA.

Input: φ (visible in simulation experiments but invisible in real quantum computing), $T, \alpha, N_{\min}, N_{\max}$;

Output: $\tilde{\varphi}$: the estimation of φ .

- 1 Initialize $\mathcal{S} = \{\tilde{\varphi}_1, \dots, \tilde{\varphi}_{N_{\min}}\}$ with N_{\min} samples using QFT-PEA with parameter T ;
 - 2 Sort \mathcal{S} from small to big;
 - 3 **while** $\#\mathcal{S} < N_{\max}$ **and** There is no subset in \mathcal{S} of length $\lfloor \alpha \#\mathcal{S} \rfloor$ and interval at most $2/T$ **do**
 - 4 Insert one more sample into \mathcal{S} while keeping \mathcal{S} sorted;
 - 5 **end**
 - 6 Remove samples from \mathcal{S} that is not in the interval;
 - 7 **return** $\tilde{\varphi} = \text{the Bayesian estimation from dataset } \mathcal{S}$;
-

Besides the QFT family, we also introduce some other quantum counting schemes.

In 2019, Suzuki et al. [SUR*19] proposed an AA-based *Maximum Likelihood Amplitude Estimation* (MLAE) algorithm. They choose an exponentially incremental sequence of M , that is, choosing $M = 2^m$ for $m \in \{0, 1, \dots, t-1\}$, estimating the probability of the amplitude with M times of Grover's iteration for N_{shot} times, and the final estimation is obtained by maximum likelihood estimation.

$$L(\tilde{\varphi}) = \prod_{m=0}^{t-1} \left[\cos^2((2^m + 1)\pi\tilde{\varphi}) \right]^{N_{\text{shot}} - h_m} \cdot \left[\sin^2((2^m + 1)\pi\tilde{\varphi}) \right]^{h_m}. \quad (24)$$

By finding the maximum of the likelihood function $L(\varphi)$ we obtain an estimation $\tilde{\varphi}$ of φ .

In 1999, Abrams et al. [AW99] proposed an AA-based algorithm for quantum amplitude estimation, and the algorithm is later called *quantum coin method* (QCoin) and numerical tested in [SH20].

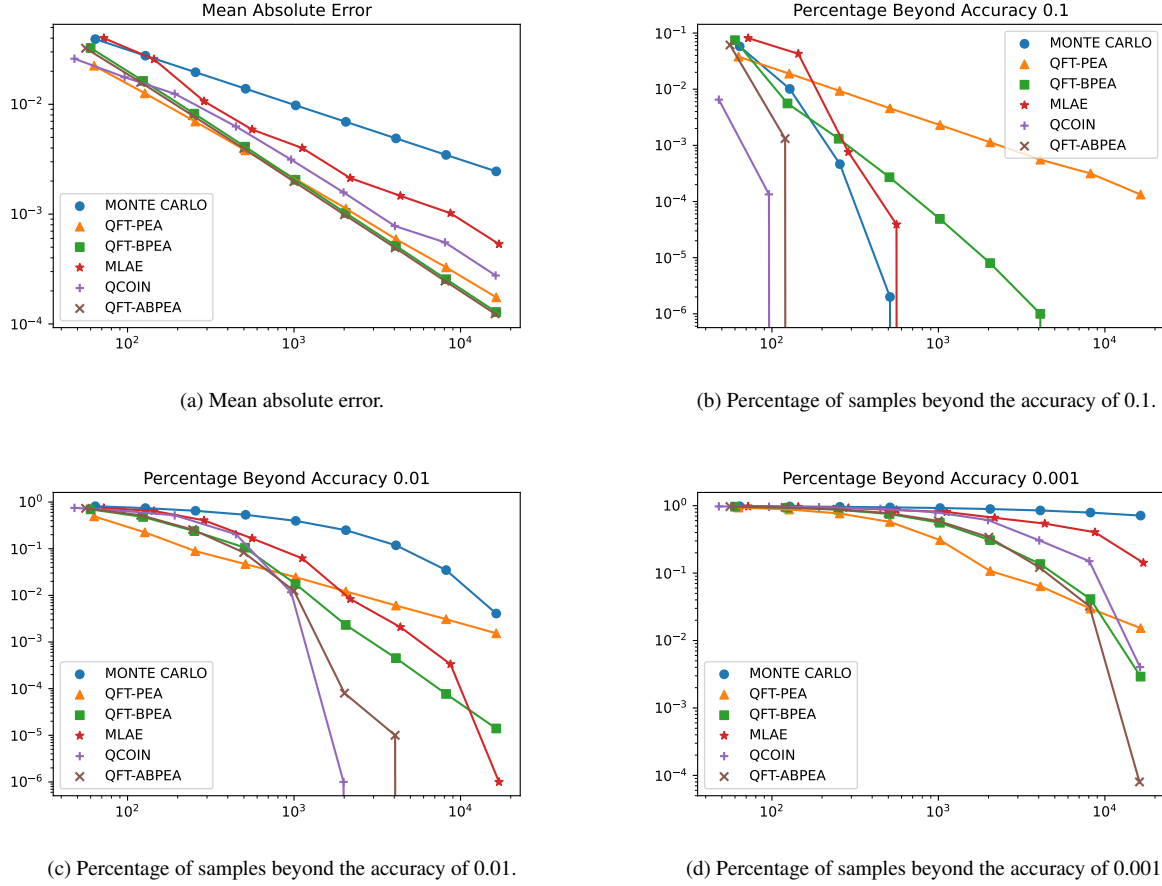


Figure 8: Quantitative evaluations on how the error scales with the number of queries to G_g (the x-axis) for each scheme.

To estimate $\varphi \in [0, 1]$ with high accuracy, they first estimate with Monte Carlo method to a smaller interval $[\varphi - \frac{\delta}{2}, \varphi + \frac{\delta}{2}]$, then remap the interval to $[0, 1 - \varepsilon]$ by amplitude amplification, and use Monte Carlo method to an even smaller interval. By using different number M of AA in each iteration, where $M = 2^m$ for $m \in \{0, 1, \dots, t-1\}$, and each iteration using N_{shot} repetitions, the information about φ is extracted with faster convergence than Monte Carlo method. It should be mentioned that QCoin method uses a different framework from other schemes above. QCoin method requires an additional step that transfers,

$$\begin{aligned} & \sum_j x_j |j\rangle |f(j)\rangle |0\rangle \\ \mapsto & \sum_j x_j |j\rangle |f(j)\rangle \left[\sqrt{1 - \left(\frac{f(j)}{2^{b-b_0}}\right)^2} |0\rangle + \left(\frac{f(j)}{2^{b-b_0}}\right) |1\rangle \right], \end{aligned} \quad (25)$$

whose accurate implementation requires 2^b extra controlled rotation gates.

To quantitatively analyze how noise scales with the number of queries in those schemes, we randomly generate 10^6 numbers uniformly between 0 and 1 as ground truths of S/N , simulate the quan-

tum counting algorithm with different schemes, and use the following statistical quantity to evaluate each scheme:

- Mean Absolute Error: to evaluate the overall noise level.
- Percentage of samples beyond the accuracy of 0.1, 0.01 and 0.001: to evaluate the level of distinct noisy dots.

The results are shown in Fig. 8. In Fig. 8(a), each quantum algorithm shows a faster error convergence than classical Monte Carlo algorithm. In Fig. 8(b)-(d) we evaluate the level of distinct noisy dots, where QCoin and QFT-ABPEA perform the best.

Next, since the distribution of $\tilde{\varphi}$ of each quantum counting scheme is relevant to φ , we do another experiment to illustrate the error pattern of each scheme. To be specific, for fixed φ s, we test each scheme for N_{test} times, then analyze the bias

$$\frac{\sum_{i=1}^{N_{\text{test}}} \tilde{\varphi}_i}{N_{\text{test}}} - \varphi, \quad (26)$$

and the mean absolute error (MAE)

$$\frac{1}{N_{\text{test}}} \sum_{i=1}^{N_{\text{test}}} |\tilde{\varphi}_i - \varphi|. \quad (27)$$

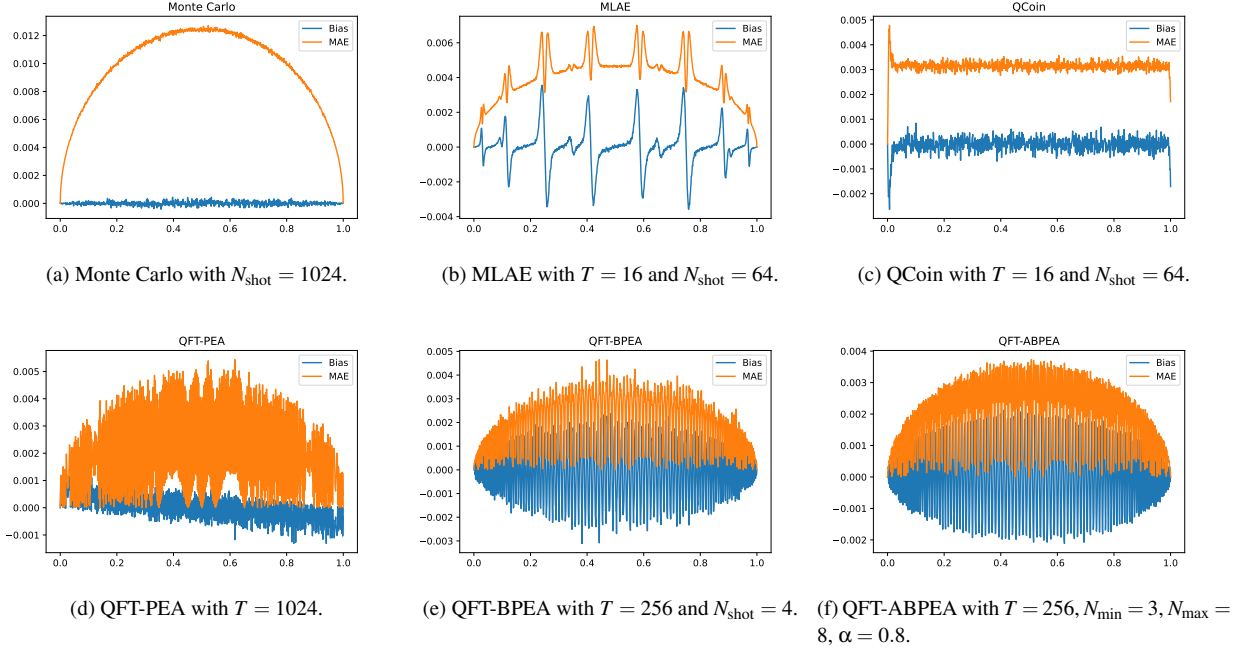


Figure 9: The error patterns of different schemes.

We choose $\phi \in \{0, 0.001, 0.002, \dots, 1\}$ and $N_{\text{test}} = 10000$. The results are shown in Fig. 9. The Monte Carlo algorithm is the only unbiased one, but has the highest MAE. The MLAE and QCoin have small bias in most area. But MLAE has bias for some special values, which can also cause fake rings like QFT-based family. And QCoin has bias and tends to give an underestimation around 0 or 1. And both them have a moderate level of MAE. The QFT-based family of algorithms have the smallest level of MAE, but the bias fluctuate greatly, which corresponds to the fake ring phenomenon.

4. Experiment

In this section, we make comparisons on real images rendered by classical path tracing and simulated quantum ray tracing with different schemes.

We use the *Blender cycles* renderer as a representation of the state-of-the-art classical ray tracing renderer. As for the quantum ray tracing result, both actual quantum computers and classical simulators available now cannot provide enough quantum memory as well as coherence time for quantum ray tracing to show its power of superposing an astronomical number of rays. Instead, we first render with a huge number of samples in Blender as the ground truth, output the colors in HDR space, and scale them into $[0, 1]$. Then we simulate the quantum noise with the same method in the pre-experiments in the scaled HDR space. Finally, we scale them back, apply tone mapping and gamma correction to obtain the SDR color, and write these colors to the image.

We use the number of intersection searching sub-procedures as the measurement of the cost. Though we can control the number of

samples per pixel and the max tracing depth D , the actual number of intersection searching can only be computed by modifying the source code of Blender, since each ray may experience different tracing depth or direct light samples. In comparison, the number of intersection searching of quantum ray tracing is completely definite, as all rays are traced as a superposition and thus share the same depth. Suppose each O_f traces the superposed rays to depth D , then one Grover's iteration G_g contains $2D$ number of intersection searching, as one G_g consists of one O_f and one O_f^{-1} . Suppose the quantum counting scheme requires N_q queries to G_g , and notice that for each pixel there are three channels (RGB), then the calculation of the color of a single pixel requires $6DN_q$ number of intersection searching.

Denote N_c to be the number of intersection searching divided by the number of pixels and D , as a measurement of the cost of classical ray tracing. Then our experiment compares the rendering result of them conditioned on

$$N_c \approx 6N_q, \quad (28)$$

as it is hard to force $N_c = 6N_q$.

We use *Blender cycles* to render a scene with 2^{20} samples per pixel to depth $D = 4$ as the ground truth, as illustrated in Fig. 10. It should be mentioned that those ray IDs only require 20 extra qubits than storing a single ray in real quantum computers. In this scene we use $b_0 = 4$ in Eq. (22), that is, each HDR color is scaled to $1/16$ before simulating the quantum random distribution. In addition, we use Blender cycles with 2^{20} samples per pixel as the ground truth, as a representation of classical ray tracing result, as shown in Fig. 11. We simulate the quantum ray tracing result, with

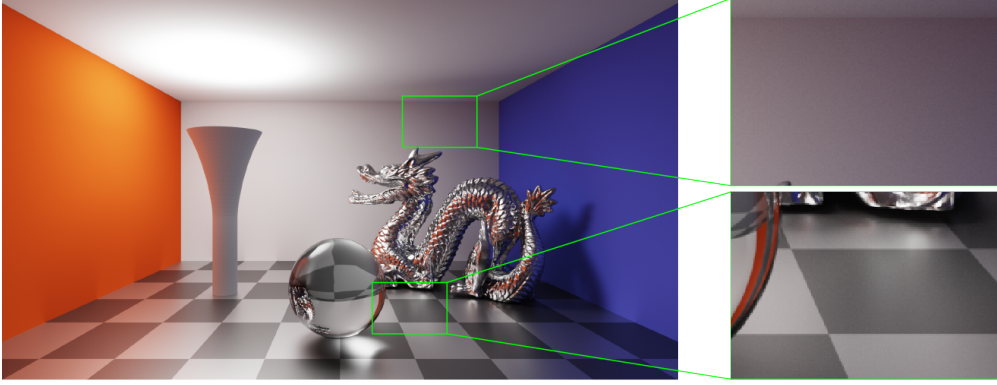


Figure 10: The ground truth, generated by Blender cycles with 2^{20} samples per pixel.

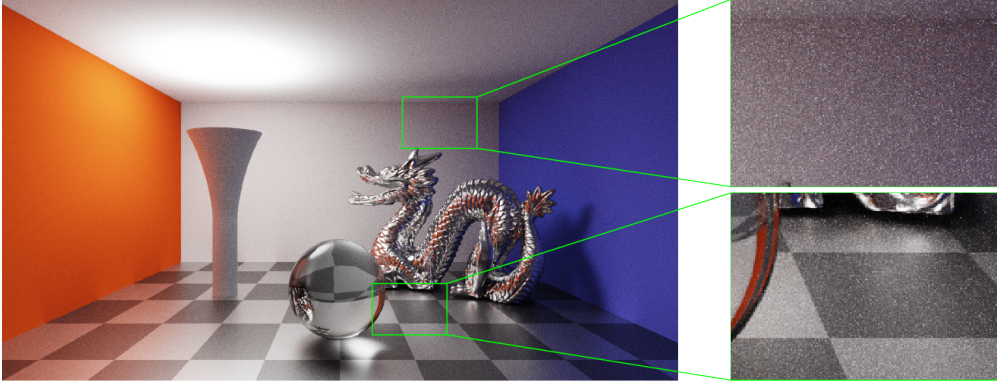


Figure 11: Classical ray tracing with 4250 sample per pixel. $N_c \approx 12186$.

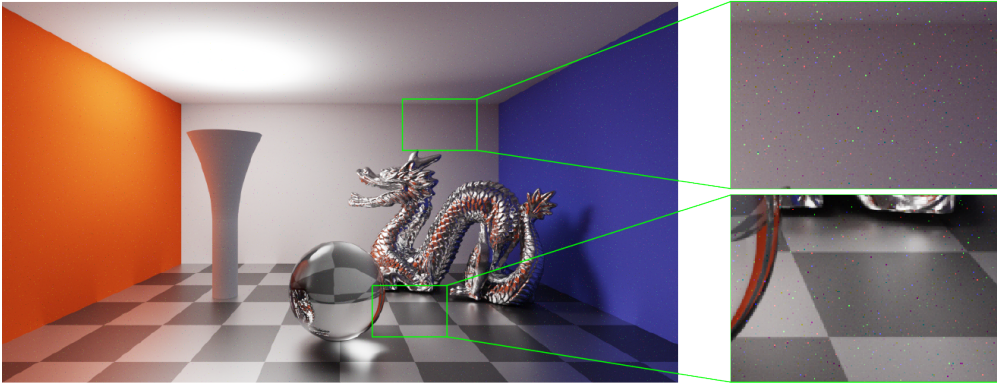


Figure 12: Quantum ray tracing result using QFT-PEA (QSS) with $T = 2048$, $N_q = 2047$.

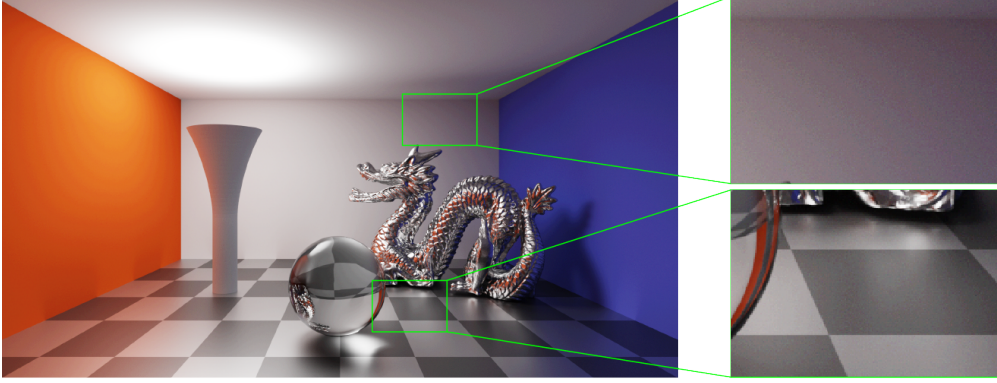


Figure 13: Quantum ray tracing using *QFT-ABPEA* with $T = 512$, $\alpha = 0.8$, $N_{\min} = 3$ and $N_{\max} = 8$, which reports $N_q = 1983$.

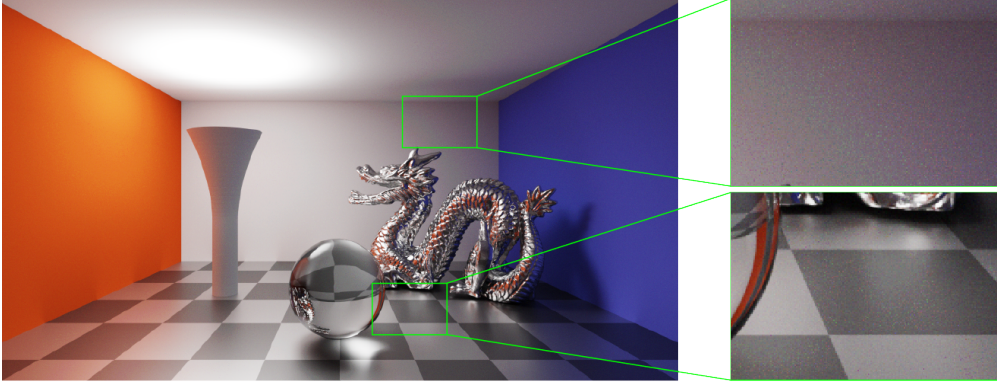


Figure 14: Quantum ray tracing using *MLAE*. $T = 32$, $N_{\text{shot}} = 64$. $N_q = 2176$.

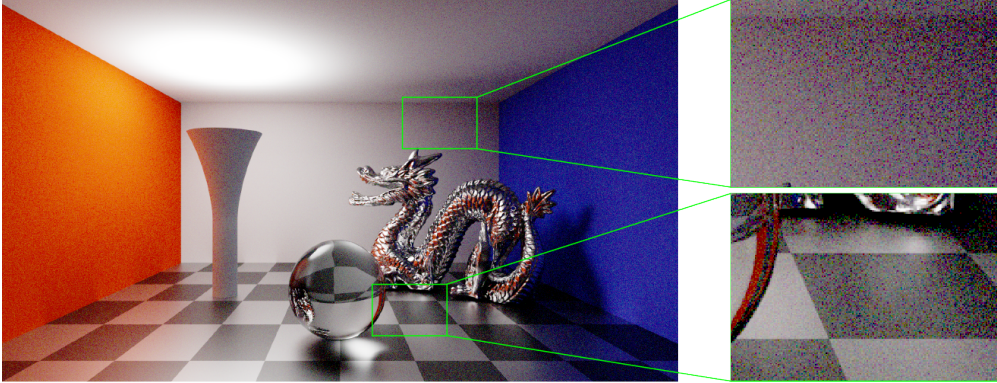


Figure 15: Quantum ray tracing using *QCoin*. $T = 32$, $N_{\text{shot}} = 64$. $N_q = 2016$.

QFT-PEA in Fig. 12, QFT-ABPEA in Fig. 13, MLAE in Fig. 14 and QCoin in Fig. 15.

In this experiment, while the classical ray tracing result is still noisy, the quantum ray tracing results can be already clean enough. The QFT-PEA result with $T = 2048$ shows many distinct noisy dots, but shows good smoothness in other area. The QFT-ABPEA result contains much slighter distinct dots, but shows slight fake rainbow-like strips. The MLAE result shows a moderate level of fake rings and smoothness. Finally, the result of QCoin shows obvious error, since the HDR color of most pixels are not exposed and thus becomes close to zero when divided by 2^{b_0} , where QCoin does not behave well as illustrated in Fig. 9.

5. Discussion

Here we discuss the limitations and potential improvements of the application of improved QSS in quantum ray tracing.

First, we claim that we are comparing quantum ray tracing and classical ray tracing by comparing the visual noise level conditioned on similar numbers of queries. In other words, we assume that the costs of performing an intersection searching in both quantum ray tracing and classical ray tracing are the same. However, classical ray tracing uses data structures like BSP tree [FKN80], KD-tree [Ben75, HH11] and BVH [Cla76] to avoid traversing all scene primitives. Meanwhile, in quantum ray tracing where an astronomical number of rays are superposed, we have to traverse all scene primitives. Besides, we do not take GPU parallel computing into consideration, which is another vital acceleration technique in classical ray tracing. In short, we may overestimate the time cost of classical ray tracing, and thus overestimate the speedup of quantum ray tracing.

Second, since the rendering equation is infinitely recursive and any cutoff on the ray tree will bring numerical truncation error, classical ray tracing utilizes Russian Roulette to ensure the unbiasedness, but in quantum ray tracing all superposed rays share the same ray tree depth, and we have no access to the intermediate information to decide the halt condition dynamically and have to predetermine a fixed ray tree, which may cause visual artifacts and must be compensated for. But in the experiments of this paper we do not simulate anything about that.

Third, quantum ray tracing only shows its power when the scene complexity is large enough. As we have addressed, the noise level of quantum ray tracing is irrelevant to the scene complexity. If a moderate level of ray samples in classical ray tracing can reduce the noise to an acceptable level, then the quantum ray tracing result with the same number of queries just brings extra noise. In real-time ray tracing where computational resources are strictly limited, quantum ray tracing may not perform better.

There are also potential improvements in our quantum ray tracing algorithm. In the current framework we only superpose the rays, and the information is extracted by phase estimation. Intuitively, the scene primitives can be another potential candidate for superposition. By leveraging minimum finding algorithm [DH96], the information of the intersection with the minimum distance can be extracted, with another quadratic speedup as well as additional er-

ror probability. However, the two frameworks work alone and cannot be directly joined, since minimum finding algorithm works in a hybrid quantum-classical way and should be implemented for each ray, where the advantage of superposing an astronomical number of rays in the current framework will fail. It will be another interesting topic to join the two frameworks to obtain a biquadratic speedup.

6. Conclusion

In the original form of QSS [Joh16], the image produced by quantum supersampling contains many detached noisy dots, as illustrated in Fig. 12. In this paper, we improve quantum supersampling for quantum ray tracing, by replacing the standard QFT-based phase with more robust quantum counting schemes like QFT-BPEA, QFT-ABPEA and MLAE. We also take another quantum counting scheme, QCoin, into comparison. We quantitatively evaluate those schemes with visual performance related evaluations, and study how they scale with the parameters of the schemes as well as their error patterns.

Finally, we build a 3D scene, use 2^{20} samples per pixel with Blender cycles renderer to generate the ground truth, and then simulate the quantum noise in the HDR linear space by sampling random numbers with respect to the theoretical distribution, to simulate the quantum ray tracing result. We show that by choosing appropriate schemes the image quality can be much better than classical ray tracing and original QSS.

References

- [AMHH18] AKENINE-MILLER T., HAINES E., HOFFMAN N.: *Real-Time Rendering, Fourth Edition*, 4th ed. A. K. Peters, Ltd., USA, 2018. 1
- [AR20] AARONSON S., RALL P.: Quantum approximate counting, simplified. In *Symposium on Simplicity in Algorithms* (2020), SIAM, pp. 24–32. 4
- [Arr17] ARRIGHETTI W.: The academy color encoding system (aces): A professional color-management framework for production, post-production and archival of still and motion pictures. *Journal of Imaging* 3, 4 (2017), 40. 5
- [AW99] ABRAMS D. S., WILLIAMS C. P.: Fast quantum algorithms for numerical integrals and stochastic processes. *arXiv* (8 1999). URL: <https://arxiv.org/abs/quant-ph/9908083v1>. 1, 3, 4, 6
- [Ben75] BENTLEY J. L.: Multidimensional binary search trees used for associative searching. *Communications of the ACM* 18 (9 1975), 509–517. URL: <https://dl.acm.org/doi/abs/10.1145/361002.361007>, doi:10.1145/361002.361007. 11
- [BHT98] BRASSARD G., HOYER P., TAPP A.: Quantum counting. *Lecture Notes in Computer Science (including subseries Lecture Notes in Artificial Intelligence and Lecture Notes in Bioinformatics)* 1443 LNCS (5 1998), 820–831. URL: <http://arxiv.org/abs/quant-ph/9805082> <http://dx.doi.org/10.1007/BFb0055105>, doi:10.1007/BFb0055105. 3, 5
- [Car12] CARAIMAN S.: Quantum computer graphics algorithms. *Buletinul Institutului Politehnic din Iasi, Sectia Automatica si Calculatoare* 62, 4 (2012), 21–38. 1
- [Cla76] CLARK J. H.: Hierarchical geometric models for visible surface algorithms. *Communications of the ACM* 19 (10 1976), 547–554. URL: <https://dl.acm.org/doi/abs/10.1145/360349.360354>, doi:10.1145/360349.360354. 11

- [CPC84] COOK R. L., PORTER T., CARPENTER L.: Distributed ray tracing. *Computer Graphics* 18 (1984), 137–145. doi:10.1145/800031.808590. 1
- [DH96] DURR C., HOYER P.: A quantum algorithm for finding the minimum. *arXiv* (7 1996). URL: <https://arxiv.org/abs/quant-ph/9607014v2>. 1, 3, 11
- [Fey82] FEYNMAN R. P.: Simulating physics with computers. *International Journal of Theoretical Physics* 1982 21:6 21 (6 1982), 467–488. URL: <https://link.springer.com/article/10.1007/BF02650179>. 2
- [Fey86] FEYNMAN R. P.: Quantum mechanical computers. *Foundations of Physics* 1986 16:6 16 (6 1986), 507–531. URL: <https://link.springer.com/article/10.1007/BF01886518>, doi:10.1007/BF01886518. 2
- [FKN80] FUCHS H., KEDEM Z. M., NAYLOR B. F.: On visible surface generation by a priori tree structures. *ACM SIGGRAPH Computer Graphics* 14 (7 1980), 124–133. URL: <https://dl.acm.org/doi/abs/10.1145/965105.807481>, doi:10.1145/965105.807481. 11
- [GGZW21] GRINKO D., GACON J., ZOUFAL C., WOERNER S.: Iterative quantum amplitude estimation. *npj Quantum Information* 2021 7:1 7 (3 2021), 1–6. URL: <https://www.nature.com/articles/s41534-021-00379-1>, doi:10.1038/s41534-021-00379-1. 3
- [Gro97] GROVER L. K.: Quantum mechanics helps in searching for a needle in a haystack. *Physical Review Letters* 79 (7 1997), 325. URL: <https://journals.aps.org/prl/abstract/10.1103/PhysRevLett.79.325>, doi:10.1103/PhysRevLett.79.325. 1, 3, 4
- [HAM19] HAINES E., AKENINE-MÖLLER T.: *Ray Tracing Gems: High-Quality and Real-Time Rendering with DXR and Other APIs*. Apress, 2019. 1
- [HH11] HAPALA M., HAVRAN V.: Review: Kd-tree traversal algorithms for ray tracing. *Comput. Graph. Forum* 30 (03 2011), 199–213. doi: 10.1111/j.1467-8659.2010.01844.x. 11
- [Joh16] JOHNSTON E. R.: Quantum supersampling. *ACM SIGGRAPH 2016 Talks* (2016). URL: <http://dx.doi.org/10.1145/2897839.2927422>, doi:10.1145/2897839. 1, 2, 4, 11
- [Kaj86] KAJIYA J. T.: The rendering equation. *Proceedings of the 13th Annual Conference on Computer Graphics and Interactive Techniques, SIGGRAPH 1986* 20 (8 1986), 143–150. doi:10.1145/15922.15902. 1
- [Kit95] KITAEV A. Y.: Quantum measurements and the abelian stabilizer problem. *arXiv* (11 1995), quant-ph/9511026. URL: <https://ui.adsabs.harvard.edu/abs/1995quant.ph.11026K/abstract>. 3
- [LU05] LANZAGORTA M., UHLMANN J. K.: Hybrid quantum-classical computing with applications to computer graphics. *ACM SIGGRAPH 2005 Courses, SIGGRAPH 2005* (7 2005). doi:10.1145/1198555.1198723. 1
- [NC02] NIELSEN M. A., CHUANG I.: Quantum computation and quantum information, 2002. 1, 3
- [SBRBN22] SANTOS L. P., BASHFORD-ROGERS T., BARBOSA J., NAVRÁTIL P.: Towards quantum ray tracing. URL: <https://arxiv.org/abs/2204.12797v1>, doi:10.48550/arxiv.2204.12797. 1, 2
- [SH20] SHIMADA N. H., HACHISUKA T.: Quantum coin method for numerical integration. *Computer Graphics Forum* 39 (9 2020), 243–257. doi:10.1111/cgf.14015. 1, 6
- [SHF13] SVORE K. M., HASTINGS M. B., FREEDMAN M.: Faster phase estimation. *Quantum Information and Computation* 14 (4 2013), 306–328. URL: <https://arxiv.org/abs/1304.0741v1>, doi:10.26421/qic14.3-4-7. 3
- [Sho97] SHOR P. W.: Polynomial-time algorithms for prime factorization and discrete logarithms on a quantum computer. *SIAM Journal on Computing* 26 (10 1997), 1484–1509. URL: <https://dl.acm.org/doi/abs/10.1137/S0097539795293172>, doi:10.1137/S0097539795293172. 1, 3
- [SKW*17] SCHIED C., KAPLANYAN A., WYMAN C., PATNEY A., CHAITANYA C. R. A., BURGESS J., LIU S., DACHSBACHER C., LEFOHN A., SALVI M.: Spatiotemporal variance-guided filtering: Real-time reconstruction for path-traced global illumination. In *Proceedings of High Performance Graphics, HPG '17*. Association for Computing Machinery, New York, NY, USA, 2017. URL: <https://doi.org/10.1145/3105762.3105770>, doi:10.1145/3105762.3105770. 1
- [SUR*19] SUZUKI Y., UNO S., RAYMOND R., TANAKA T., ONODERA T., YAMAMOTO N.: Amplitude estimation without phase estimation. *Quantum Information Processing* 19 (4 2019). URL: <http://arxiv.org/abs/1904.10246><http://dx.doi.org/10.1007/s11128-019-2565-2>, doi:10.1007/s11128-019-2565-2. 3, 4, 6
- [TTK09] TAKAHASHI Y., TANI S., KUNIHIO N.: Quantum addition circuits and unbounded fan-out. *Quantum Information and Computation* 10 (10 2009), 872–890. URL: <https://arxiv.org/abs/0910.2530v1>, doi:10.26421/qic10.9-10-12. 3, 5
- [WG16] WIEBE N., GRANADE C.: Efficient bayesian phase estimation. *Physical Review Letters* 117 (6 2016), 010503. URL: <https://journals.aps.org/prl/abstract/10.1103/PhysRevLett.117.010503>, doi:10.1103/PHYSREVLETT.117.010503/FIGURES/5/MEDIUM. 3
- [Whi80] WHITTED T.: An improved illumination model for shaded display. *Communications of the ACM* 23 (6 1980), 343–349. URL: <https://dl.acm.org/doi/abs/10.1145/358876.358882>, doi:10.1145/358876.358882. 1
- [Wie19] WIE C. R.: Simpler quantum counting. *Quantum Information and Computation* 19 (7 2019). URL: <https://arxiv.org/abs/1907.08119><http://dx.doi.org/10.26421/QIC19.11-12>, doi:10.26421/QIC19.11-12. 3
- [ZLY*21] ZENG Z., LIU S., YANG J., WANG L., YAN L.-Q.: Temporally reliable motion vectors for real-time ray tracing. *Computer Graphics Forum* 40, 2 (2021), 79–90. doi:https://doi.org/10.1111/cgff.142616. 1